WISC

UNIVERSITY OF WISCONSIN • MADISON, WISCONSIN

PLASMA PHYSICS

MEASUREMENT OF MAGNETIC FLUCTUATION-INDUCED HEAT TRANSPORT IN TOKAMAKS AND RFP

G. Fiksel,* Roger D. Bengtson,[a] M. Cekic, D. Den Hartog, S.C. Prager, P. Pribyl,[b] J. Sarff, C. Sovinec, M.R. Stoneking, R.J. Taylor,[b] P.W. Terry, G.R. Tynan,[b] A.J. Wootton[a]

DOE/ER/54345-276 July 1996

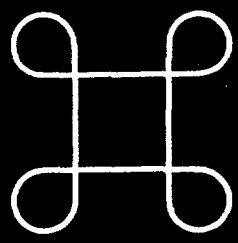

DNSIN

* Invite

) University ex stin
) titute o m Fusion Rese

NOTICE

Printed in the United States of America
Available from
National Technical Information Service
U.S. Department of Commerce
5285 Port Royal Road
Springfield, VA 22161

NTIS Price codes
Printed copy: A02
Microfiche copy: A01

DOE/ER/54345--276

Measurement of Magnetic Fluctuation-Induced Heat Transport in Tokamaks and RFP

G. Fiksel,* Roger D. Bengtson,[a] M. Cekic, D. Den Hartog, S.C. Prager, P. Pribyl,[b] J. Sarff, C. Sovinec, M.R. Stoneking, R.J. Taylor,[b] P.W Terry, G.R. Tynan,[b] A.J. Wootton[a]

Department of Physics
University of Wisconsin - Madison,
Madison, WI 53706, USA

Presented at 23rd EPS Conference on Controlled Fusion and Plasma Physics, Kiev, Ukraine, 24-28 June 1996.

* Invited speaker.

a) University of Texas, Austin

b) Institute for Plasma and Fusion Research, UCLA.

Abstract

The local electron energy flux produced by magnetic fluctuations has been measured directly in the edge plasma ($r/a > 0.75$) of the Madison Symmetric Torus (MST) [R.N. Dexter *et al.*, Fusion Technology **19**, 131 (1991)] reversed field pinch (RFP), Continuous Current Tokamak (CCT) [R.J. Taylor *et al.*, Phys. Rev. Lett. **63**, 2365 (1989)], and the scrape-off layer of the TEXT-U tokamak [K.W. Gentle, Nucl. Technol. Fusion **1**, 479 (1981)]. The flux, produced by electrons traveling parallel to a fluctuating magnetic field, is obtained from correlation between the fluctuations in the parallel heat flux and the radial magnetic field. The fluctuations in the parallel heat flux were measured with a fast insertable pyrobolometer. The measurements reveal fundamental differences in the nature of electron energy transport in the RFP and the tokamak. In the RFP the fluctuation induced energy flux is large ($\sim$100 kW/m^2, comparable to the total Ohmic heating power) inside the reversal surface where the magnetic field is expected to be stochastic, and small in the edge. The magnetic fluctuation induced radial energy flux Q and radial particle flux Γ (measured independently) are related by a "convective" formula $Q \approx 3/2T\Gamma$. The electron heat transport is significantly lower than predicted by the Rechester-Rosenbluth transport model. This feature of the electron energy transport can be explained using self-consistent calculations that account for clumping of electrons streaming along the magnetic field. In the tokamak the magnetic fluctuations do not contribute to the total energy transport except in the vicinity of the $q = 2$ magnetic surface, where the transport is associated with large amplitude Mirnov oscillations.

I. INTRODUCTION

It has long been recognized that fluctuations in the magnetic field are a potent mechanism for the anomalous transport of energy in confined plasmas [1].The energy transport process originates from particle motion along magnetic fields, which have a fluctuating component in the radial direction (perpendicular to the confining equilibrium magnetic surfaces). A key feature is that the transport can be large even if the fluctuation amplitude is small. If the fluctuations are resonant with the equilibrium magnetic field (i.e., the fluctuation amplitude is constant along an equilibrium field line) then a small fluctuation can introduce stochasticity to the field line trajectories. Particles following the chaotically wandering field lines can rapidly carry energy across the plasma.

After several decades of research it has remained an open question as to whether magnetic fluctuations are responsible for anomalous transport in confinement systems, such as the tokamak, stellarator, and reversed field pinch. In all these devices, magnetic fluctuations have been measured and anomalous energy transport is observed. However, causality between the two has never been proved or disproved. Lacking direct measurements of the energy flux driven by magnetic fluctuations, inferences have been made from measurements of the magnetic fluctuation amplitude. For example, under an assumption of collisionless electrons in a stochastic magnetic field a simple quasilinear estimate [2,3] of the electron thermal conductivity is often applied to experiment

$$\chi_e = v_e L_c \tilde{b}_r^{\,2} \qquad (1)$$

where v_e is the electron thermal velocity, L_c s the parallel correlation length for the magnetic fluctuations, and $\tilde{b}_r = \tilde{B}_r / B$ is their relative amplitude. This heuristic estimate (customarily referred to as the Rechester-Rosenbluth model) usually results in small magnetic-field-induced transport at the plasma edge, as concluded in TEXT-U [4]. On the other hand, the level of fluctuations may become significant deeper in the plasma core [3, 5]; experiments with a variable safety factor q in the TOKAPOLE tokamak- [6] indicate that magnetic fluctuations are significant at low q. Experiments in the ISX-B tokamak [7] at high beta (plasma pressure), Doublet III [8], and JET [9] show a correlation between confinement time and magnetic fluctuations. As the confinement time decreases, the fluctuations increase; however, causality between them was not established.

Magnetic fluctuations in the RFP have even larger amplitudes than in a tokamak. Large amplitude tearing modes are resonant in the core and the amplitudes of the fluctuations exceed the magnetic islands overlap condition, therefore establishing a stochastic magnetic field in the core.

In this paper we present direct *measurements* of magnetic fluctuation induced electron heat transport in the Madison Symmetric Torus (MST) [10] RFP, Continuous Current Tokamak (CCT) [11] and TEXT-U [12] tokamak. The paper is organized as follows. The description of the diagnostic is given in

Section II. The RFP studies are described in Section III. The tokamak studies are described in Section IV. The discussion of the results can be found in Section V.

II. DIAGNOSTIC

To determine decisively the role of magnetic fluctuations in energy transport requires measurement of the energy flux specifically generated by the fluctuations. The radial energy flux arising from electron motion parallel to the magnetic field is given by $Q_r = Q_{||} \cdot \hat{r} = (Q \cdot \hat{b})(\hat{b} \cdot \hat{r})$ where $\hat{b}$ and $\hat{r}$ are unit vectors along the magnetic field and the radial direction respectively. Separating Q and $\hat{b}$ into equilibrium and fluctuating quantities yields the ensemble-averaged radial energy flux [13]

$$Q_r = \frac{\langle \tilde{Q}_{||} \tilde{B}_r \rangle}{B} \qquad (2)$$

where $\tilde{Q}_{||}$ is the fluctuating electron heat flux parallel to the equilibrium magnetic field (i.e., $\tilde{Q}_{||} = \int v_{||}(mv^2/2)\tilde{f}(v)dv$), $\tilde{B}_r$ is the fluctuating radial magnetic field, B is the equilibrium field, and the brackets < > represent the flux surface averaged product of fluctuating quantities. The key to measuring the energy flux from the fluctuating magnetic field is to obtain $\tilde{Q}_{||}$ and $\tilde{B}_r$ locally within the plasma and correlate these two quantities. This approach differs from all past work in which transport is *calculated* using the Rechester-Rosenbluth transport model with the measured $\tilde{B}_r$ as input.

While local measurements of $\tilde{B}_r$ can be readily obtained (for example, with a small pickup coil) fast measurement of $\tilde{Q}_{||}$ in a plasma environment can be quite challenging. In order to measure $\tilde{Q}_{||}$ we have devised the fast bolometer technique described in references [14,15] The technique was used for magnetic fluctuation induced heat flux measurements in MST RFP [16], TEXT-U tokamak [17], and CCT tokamak [18].

The schematics of the bolometer is shown in Fig. 1. The bolometer incorporates pyrocrystals of $LiNbO_3$ for the heat flux measurements. The diameter of the crystal is 1 cm and the thickness is 1 mm. When exposed to a plasma (or any other source of thermal energy) the crystal generates electric current that is proportional to the absorbed power. The signal is measured with a fast current-to-voltage converter. The heat flux measurements were absolutely calibrated and the frequency bandwidth was measured to be 150 kHz [14]. The sensitivity of the bolometer is 1.8×10^{-8} A/W. The range of measurable fluxes is 0.1 W/cm^2 - 10 kW/cm^2. The bolometer housing also

contains a small magnetic coil for radial magnetic field measurements. The frequency bandwidth of magnetic measurements was 200 kHz [15].

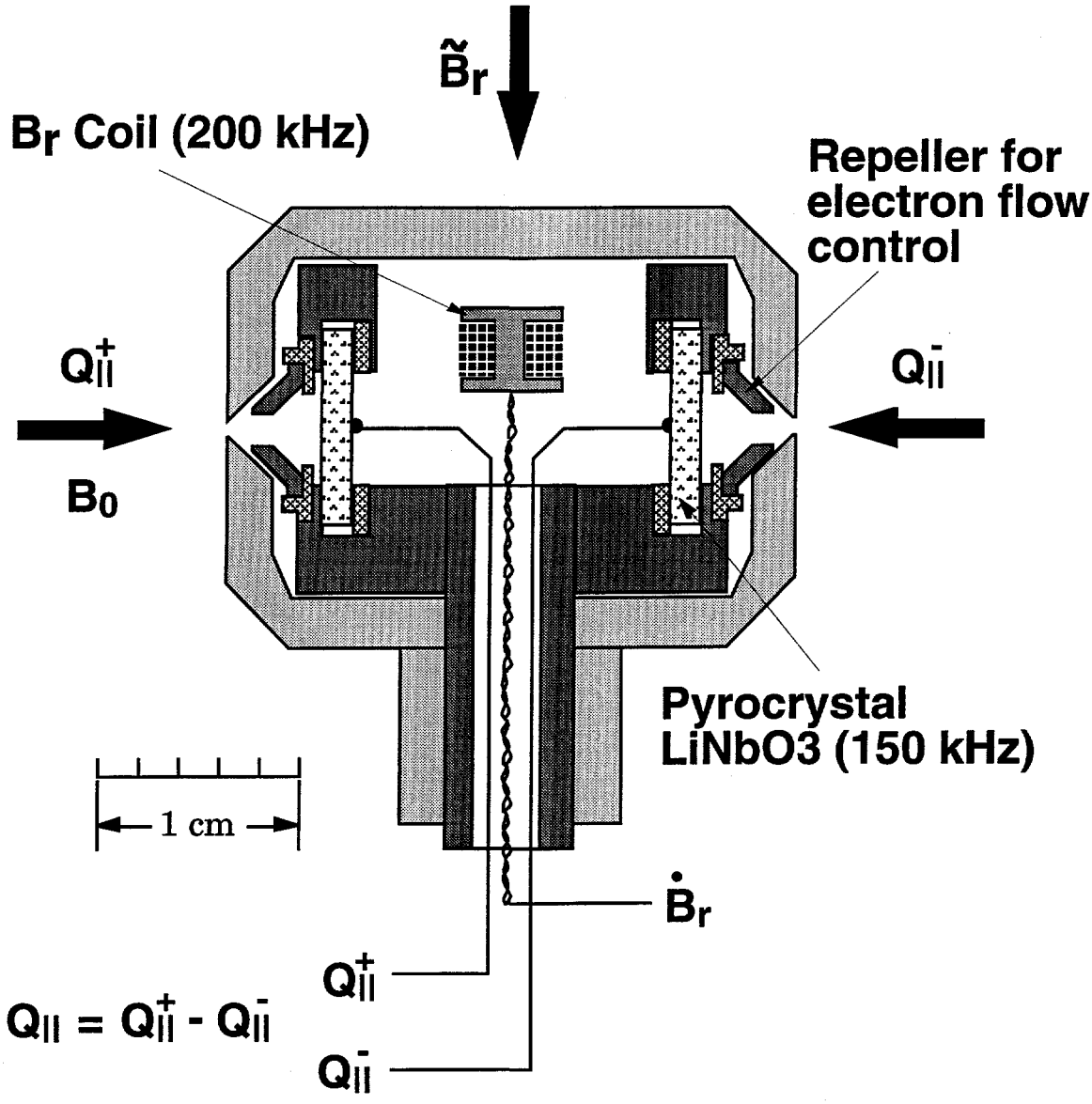

Figure 1. A cutaway view of the bolometer showing the elements and illustrating the measurements.

The main source of the heat flux at the plasma edge is electrons streaming along the magnetic field lines. The electrons enter the bolometer through small, thin apertures of 1 mm diameter in the protective boron nitride shroud. There are two apertures located on the opposite sides of the shroud. When the bolometer is aligned along the magnetic field it measures the field-aligned heat flux simultaneously in two opposite directions. These heat fluxes are subtracted from each other in order to yield the net parallel heat flux. This approach allows one, in addition, to subtract the plasma noise signals (found to be small) and the radiation power (also found to be small in comparison to the direct electron power flux). In addition, we can control the electron flow by biasing the repeller electrode. Applying a negative bias of 1 kV essentially shuts off the electron flux and greatly reduces the total energy deposited into the bolometer during a discharge. Reducing the bias to 0 V allows the electrons to enter the bolometer. In the experiments described below the bolometer is open during of 2-8 ms during the plasma current flat-top. The bolometer collects all electrons with energy up to ~1-2 keV when the electron gyroradius becomes comparable to the entrance aperture radius. The geometrical transparency of the entrance aperture was evaluated by a Monte-Carlo simulation of the incoming electron flux in the magnetic field. The ions enter the bolometer as well and are not explicitly separated, but their heat flux is smaller by at least a factor of $(m_e / M_i)^{1/2}(T_i / T_e)^{1/2}$ in comparison to the electron flux.

The separation of the entrance apertures in the parallel direction was 2.5 cm, which determines the parallel wavelength resolution. The magnetic coil diameter was 0.5 cm and the length (perpendicular to the magnetic field) 0.3 cm. These spatial dimensions appear to be much smaller than the characteristic parallel and perpendicular correlation lengths and wave length of interest for both RFP and tokamaks. For example, the parallel correlation length for the dominant m = 1 tearing mode in MST [16] and m/n = 2/1 Mirnov oscillation in the CCT [17] is ~0.5-1 m. The perpendicular correlation length for dominant modes is about 10 cm for MST and 4-8 cm for CCT.

III. RFP MEASUREMENTS

MST is a relatively large RFP (a = 0.5 m, R = 1.5 m) with moderate plasma current (I < 0.5 MA). To permit diagnostic insertion into the plasma, the plasma was maintained at reduced parameters. For measurements at the plasma edge ($r / a > 0.9$) the plasma current was maintained at 220 kA; for deeper insertion ($0.75 < r / a < 0.9$) the current was reduced to 120 kA. The line-averaged density was 0.8 - 1 x 10^{13} cm^{-3}, and the central electron temperature was 100 - 150 eV. The confinement properties and fluctuation characteristics are relatively unchanging over the full current range of MST, so that we believe that the results are not peculiar to low current. Magnetic fluctuations have been studied extensively in MST [19,20]. Nearly all the fluctuation power (> 90%) resides in several modes at low frequency (f < 30 kHz) with poloidal and toroidal mode number m = 1 and n = 5 - 8. Detailed

comparison between the nonlinear MHD computation and experimental measurements, including details of nonlinear coupling [21], has established that the fluctuations are nonlinearly coupled, global, tearing modes resonant in the core. These modes have large amplitude of $\tilde{B}_r/B \sim 1\text{-}2\%$ and are capable of breaking the magnetic surfaces within the reversal surface [22] (at $r/a \approx 0.85$) . This provides an ideal environment for fluctuation induced transport studies. The higher frequency fluctuations (f > 50 kHz) are small scale turbulence resonant with the local magnetic field. Their origin is not yet established.

The radial energy flux driven by magnetic fluctuations is obtained from the fluctuation measurements by forming the correlated product $<\tilde{Q}_{\|}\tilde{b}_r>$. The flux surface average < > is realized experimentally by averaging many time records. Since the phase of the fluctuations is random over a magnetic surface, the ensemble average approximates a magnetic surface average. The product can be decomposed into spectral components:

$$Q_r = B^{-1}\sum_f |\tilde{Q}_{\|}(f)||\tilde{B}_r(f)|\gamma(f)\cos[\phi(f)] \qquad (2)$$

where $|\tilde{Q}_{\|}(f)|$ and $|\tilde{B}_r(f)|$ are the average spectral amplitudes of the two fluctuating quantities, $\gamma(f)$ is the cross-coherence, and $\phi(f)$ is the phase shift between the fluctuating electron heat flux and the fluctuating radial magnetic field. The spectral amplitudes, cross-coherence, and the phase shift were calculated using the fast Fourier transform (FFT) technique. To cross-check the calculations the transport was also calculated using direct time averaging. The statistical analyses of our data showed a very good agreement between the direct time averaging and the spectral analyses.

The frequency spectra of $\tilde{B}_r$ and $\tilde{Q}_{\|}$ shown in Fig. 2a exhibit peaking at low frequency. The peak at the extreme low end of the bandwidth represents the sawtooth oscillations. The gentle peak apparent at about 10 kHz in both signals arises from the tearing oscillations.

To determine the radial energy flux driven by these fluctuations we have evaluated the cross-coherence between $\tilde{Q}_{\|}$ and $\tilde{B}_r$ from ensembles of 60 - 120 reproducible discharges. The magnitude and phase of the cross-coherence is displayed in Figures 2b and 2c (for r/a = 0.75). The peak coherence is strong and restricted to low frequency (≈ 10 kHz). This coherence arises from the several dominant tearing fluctuations. The coherence decreases with radius, reaching ≈ 0.2 at r/a = 0.85 (reversal surface) and ≈ 0.3 near r/a = 0.95. The cross-power frequency spectrum is displayed in Fig. 2d. It is clear that the energy flux from magnetic fluctuations arises mainly from

the low frequency tearing oscillations resonant in the core. The higher frequency microturbulence has a weak cross-coherence and low amplitude; hence, it does not contribute significantly to the energy flux from magnetic fluctuations. The cross-phase at the frequency of maximum coherence is about 60 degrees, not optimal for transport. However, the resulting energy flux can be large since the fluctuation amplitudes are large.

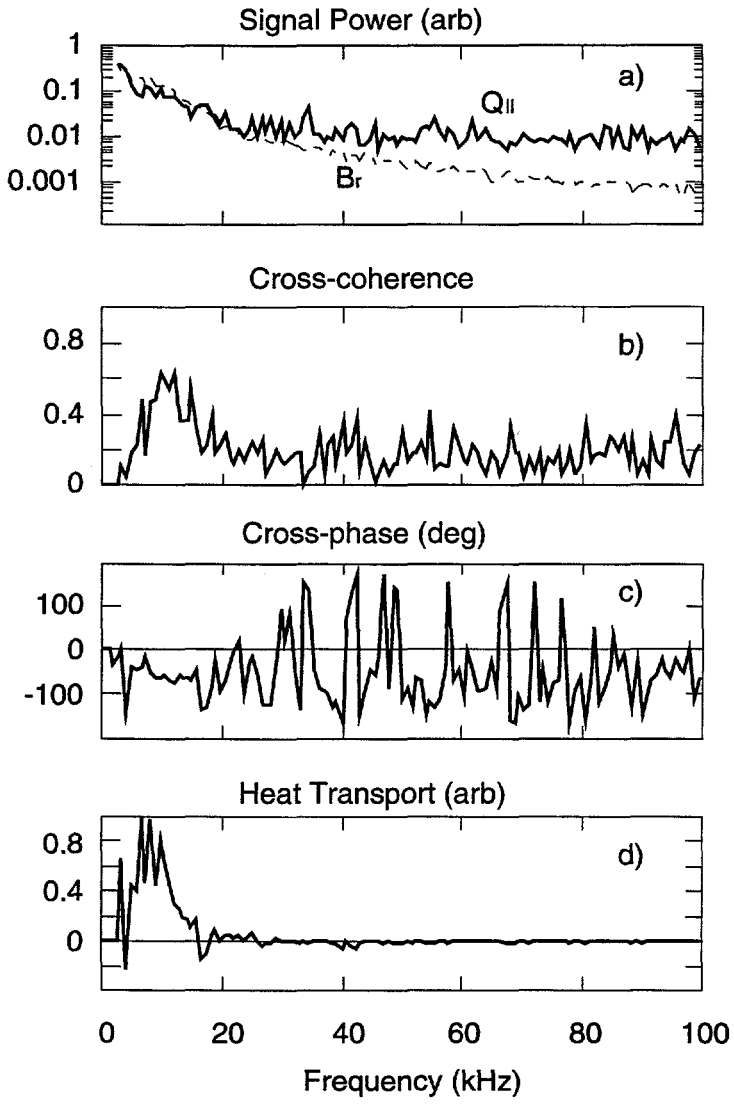

Figure 2. RFP frequency spectra of a) fluctuation of $Q_{||}$ and B_r; b) cross coherence of $Q_{||}$ and B_r, c) cross phase, and d) heat transport.

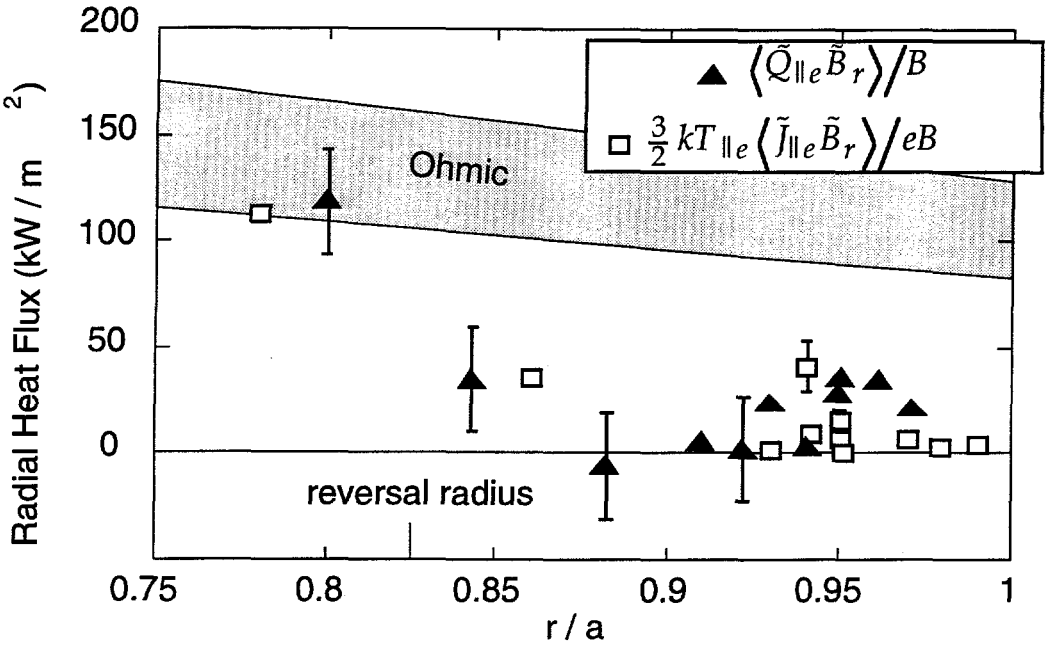

Figure 3. Radial profile of magnetic fluctuation induced heat transport in RFP $Q_r = \langle \tilde{Q}_{\parallel} \tilde{B}_r \rangle / B$ (solid triangles), and particle transport $\Gamma_r = \langle \tilde{\Gamma}_{e\parallel} \tilde{B}_r \rangle / B$ multiplied by $3/2kT_e$. Also shown the total energy flux density calculated as the total Ohmic power normalized to the magnetic surface area at the corresponding radius.

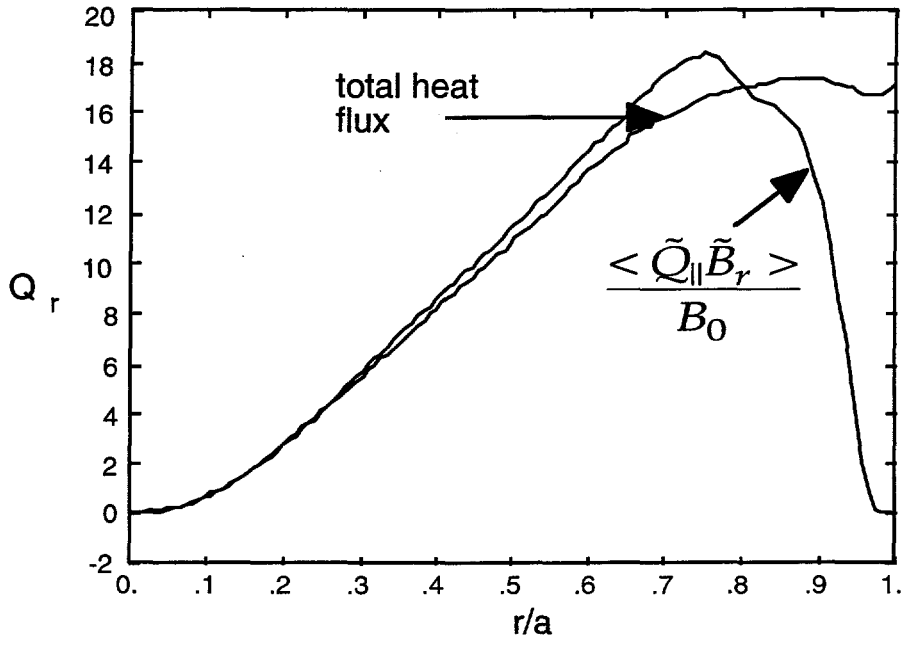

Figure 4. Results of DEBS code simulation of magnetic fluctuation induced heat transport in RFP.

The radial profile of the energy transport $Q_r = \langle \tilde{Q}_{\|} \tilde{B}_r \rangle / B$, is shown in Fig. 3 (solid symbols). Also shown is the total energy flux density calculated as the total Ohmic power normalized to the magnetic surface area at the corresponding radius. We see that at the plasma edge the heat transport from magnetic fluctuations is low, but inside the reversal surface ($r/a < 0.85$) it constitutes a significant fraction of the total flux. The observed radial dependence of the anomalous transport is consistent with expectation of field line stochasticity inside the reversal surface. The edge magnetic surfaces are not similarly disturbed since the tearing fluctuations are not resonant in that region.

These implications agree with results of MHD simulations using the nonlinear resistive MHD code DEBS [23] with finite electron pressure. The parallel electron heat flux was simulated in the conductive approximation as $Q_{\|} \propto n \nabla_{\|} T_e$ and the magnetic heat transport $\langle \tilde{Q}_{\|} \tilde{b}_r \rangle$ was calculated. The results of these simulations are shown in Fig. 4. The magnetic fluctuation induced heat flux reached its maximum and becomes comparable to the total heat flux just inside the reversal surface.

The stochastization of the magnetic field is expected to increase the particle transport as well as the heat transport. The magnetic fluctuation induced electron flux $\Gamma_r = \langle \tilde{\Gamma}_{e\|} \tilde{B}_r \rangle / B$ was measured independently by correlating the fluctuation of parallel electron flux $\tilde{\Gamma}_{e\|} = \tilde{J}_{e\|} / e$ and the radial magnetic field $\tilde{B}_r$. The parallel electron current $\tilde{J}_{e\|}$ was measured with a small insertable electron energy analyzer (EEA) [24]. The radial profile of the particle transport Γ_r multiplied by $3/2kT_e$, is shown in Fig. 3 on the same scale as the heat flux. It is evident that both heat and particle transport are comparable and exhibit similar radial dependence.

From the analysis of the radial energy and particle flux two important conclusions can be made. These conclusions are summarized as follows:

1. *The electron heat flux is convective.* This conclusion stems from the above mentioned comparison $\Gamma_r = 3/2kT_e Q_r$.

2. *The electron heat flux is ambipolar.* In other words, the electron heat transport is described by the Rechester-Rosenbluth (RR) model but with the ion speed substituted into Eq. 1 rather than the electron speed. Indeed, the magnetic fluctuation amplitude is large so the RR estimate (Eq. 1) would give unrealistically large heat fluxes. Nevertheless, if the ion speed substituted into Eq. 1 rather than the electron speed then the estimate would agree with experiment. Estimating $Q_r = T_e / a_T n_e \chi_e$, where a_T is the characteristic electron temperature gradient scale length and $\chi_e = v_e L_c \tilde{b}_r^2$, yields $\chi_e \approx 2000$ m^2/s (for $T_e = 150$ eV, $L_c = 1.5$ m and $\tilde{b}_r = 1.5\%$), and $Q_r \approx 1700$ kW/m^2 (for $n_e = 0.7 \times 10^{19}$ m^{-3} and $a_T = 0.2$ m) which is about a

factor of 16 larger than the measured flux. Substituting the ion speed at the same temperature would result in $\chi_e \approx 50\,\mathrm{m^2/s}$, and $Q_r \approx 40\,\mathrm{kW/m^2}$, which is only about a factor of 2-3 smaller than the measured flux. Similarly, estimates of the diffusion coefficient through the measured energy confinement time for MST [25] $\tau_E = 1$ ms result in $\chi_e = a^2 / 4\tau_E = 50\,\mathrm{m^2/s}$ for $a = 0.5$ m. We will discuss these conclusions in more detail in Section V.

IV. Tokamak Measurements

Measurements of magnetic fluctuation induced electron heat transport were performed in the CCT tokamak [18] and TEXT-U Tokamak [17]. We start with the CCT experiments since more detailed radial profile information was obtained. The comparatively low-temperature and low-density CCT plasma tolerates probe insertion quite well without any adverse effect, as was established by numerous probe experiments in this machine. Hence, we obtained detailed profile information. The TEXT-U measurements were made only in the scrape-off layer.

The CCT plasma has a major radius $R = 1.5$ m and minor radius $a = 0.36$ m. In the described experiments the plasma current $I_p = 40$ kA, the toroidal magnetic field $B_T = 0.25$ T, the safety factor at the edge $q(a) = 2.6\text{->}3$, and the line averaged density $n_e = 2.5\times10^{12}\,\mathrm{cm^{-3}}$. After proper conditioning at the plasma edge we could insert the bolometer as deep as $r / a = 0.75$ without change in discharge parameters such as loop voltage, plasma current, plasma density, visible and UV radiation, magnetic activity, and plasma position. The extent of the insertion was limited by the bolometer damage rather than plasma perturbation.

The same data analysis technique was used for tokamaks as for the RFP. Typically, ten shots were taken at each radial location. The signals were recorded during 8 ms at the CCT discharge flat-top period at a sampling rate of 1 μs.

Typical frequency spectra of the parallel heat flux and the radial magnetic field are shown in Fig. 5. The magnetic spectrum features a high amplitude low-frequency coherent peak (Mirnov oscillation) centered at ≈ 5 kHz and low amplitude broadband high frequency fluctuations. In order to differentiate between them we draw a separation line at 20 kHz. The radial profile of the fluctuations amplitudes are shown in Fig. 6. In addition, the equilibrium (dc) value of the parallel heat flux is shown.

The 8 ms pulse was separated into 16 realizations at 0.5 ms each. Therefore, we had 160 experimental realizations per radial location for statistical analyses. Fig. 7 shows the cross-coherence $\gamma(f)$ and the phase shift $\phi(f)$ at the probe radial position of 29 cm. The statistical noise level of the cross-coherence is shown by the thin solid line.

The energy flux produced by broadband (f > 20 kHz) magnetic turbulence is very small. The transport evaluated from Eq. (2) for these frequencies is shown in Fig. 8. We compare this flux with the total energy

flux, approximated by the ratio of the total Ohmic input power to the plasma surface area, which results in about 0.2 W/cm^2. The broadband turbulence induced flux is about 2 % of the total flux. The small contribution is mostly a result of the relatively small fluctuation amplitude; even if $\tilde{Q}_{\|}$ and $\tilde{B}_r$ were perfectly coherent ($\gamma = 1$) and in phase ($\cos\phi = 1$), the fluctuation induced flux would still only contribute 10 % of the total energy flux.

The coherent Mirnov oscillations have a high amplitude and can cause substantial radial transport. The amplitude of the oscillations varies significantly from shot to shot as well as within the 8 ms gate time. Since the magnetic transport is expected to depend on the magnetic fluctuation amplitude the 160 realizations at each radial location were grouped according to the corresponding fluctuation amplitude. Accordingly, the corresponding radial energy transport was calculated. The radial profile of the energy transport at the magnetic fluctuation amplitude of $\tilde{B}_r / B_0 = 7 \times 10^{-4}$ is shown in Fig. 9.

The radial transport is strongly peaked at r = 29 cm ($r/a = 0.8$). Analysis of the oscillations using magnetic pickup coil arrays located at the wall indicates the dominant mode of the Mirnov oscillation for the conditions of the experiment is $m/n = 2/1$ although other modes (3/1, 3/2) were present. No quantitative mode analysis at the probe location has been made. The location of the peak coincides with the estimated position of $q = 2$ rational surface. Estimate of the width of the m = 2 island (using the measured $\tilde{b}_r$) gives $w = 4(\tilde{b}_r R q^2 / m q')^{1/2}$ = 6–7 cm and agrees well with the width of the measured energy flux profile. An interesting feature is that transport is low (~ 5% of the total energy flux) away from the $q = 2$ surface even though the $m = 2$ amplitude stays large (see Fig. 6b). The reduction in transport occurs mainly from the change in the phase shift between $\tilde{Q}_{\|}$ and $\tilde{B}_r$, from $\approx 60°$ at the peak to $\approx 90°$ (out of phase) outside of the peak.

The dependence of the energy flux, measured at the radius of the maximum of energy transport, on the fluctuation amplitude is shown in Fig. 10. The flux increases monotonically with fluctuation amplitude. At the lowest amplitude the flux is zero within the error bars, which are represented by the points scatter. At the largest amplitude, the flux (at the maximum) is comparable to the total energy flux.

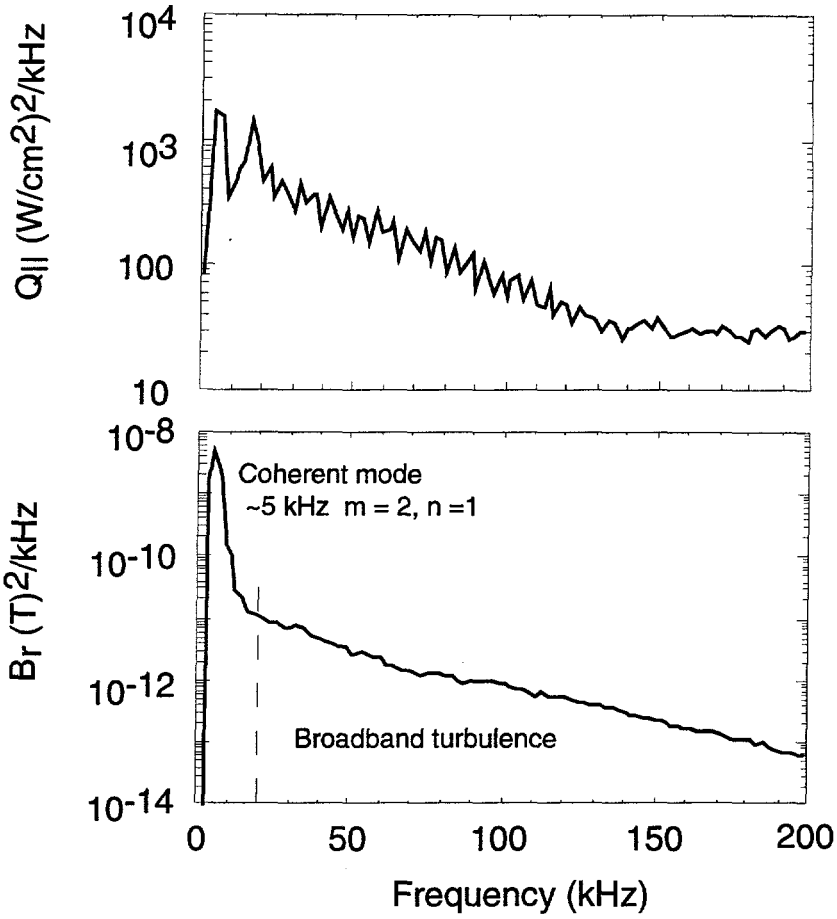

Figure 5. Frequency spectra of the fluctuations of the parallel electron heat flux (a) and radial magnetic field (b) in CCT tokamak. The vertical dashed line at 20 kHz separates broadband turbulent fluctuations and low frequency coherent modes.

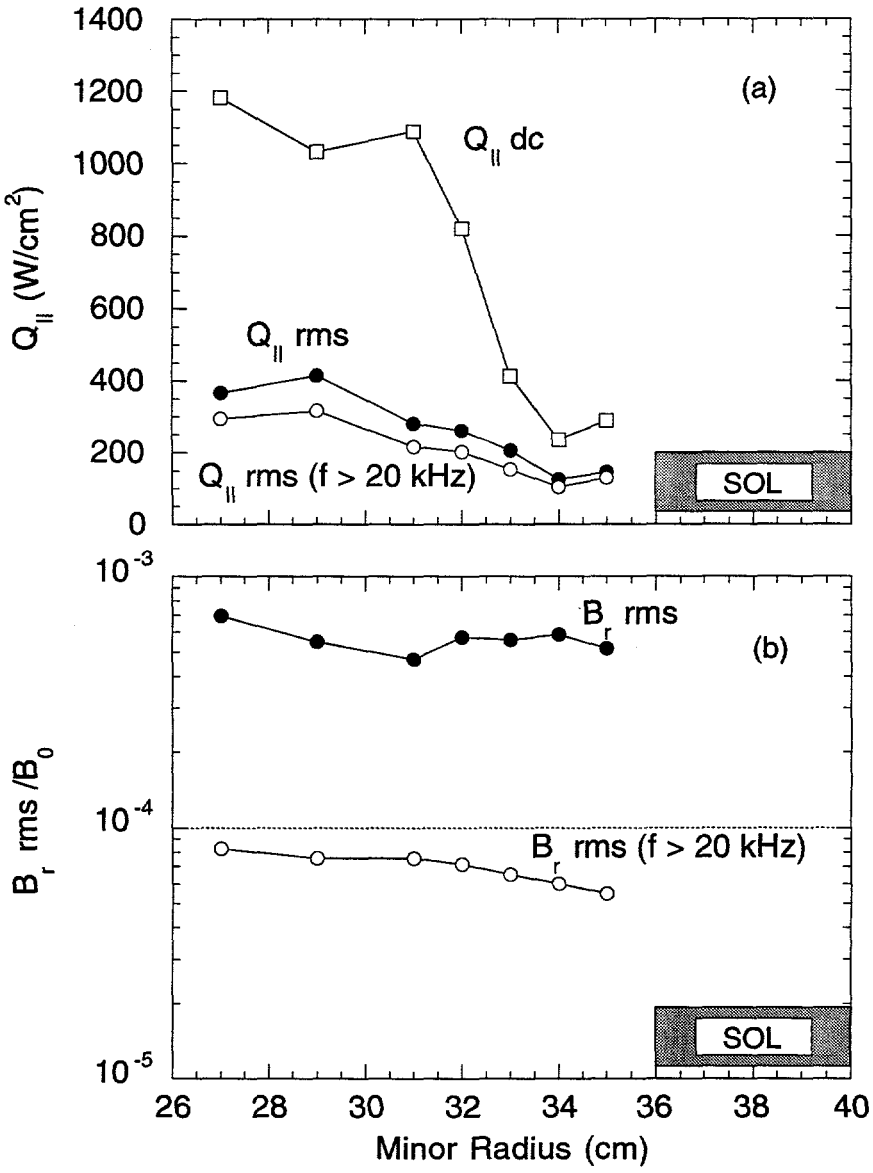

Figure 6. Radial profile of fluctuations amplitudes of the parallel electron heat flux (a) and radial magnetic field (b) in CCT. The equilibrium (dc) value of the parallel heat flux is shown for comparison.

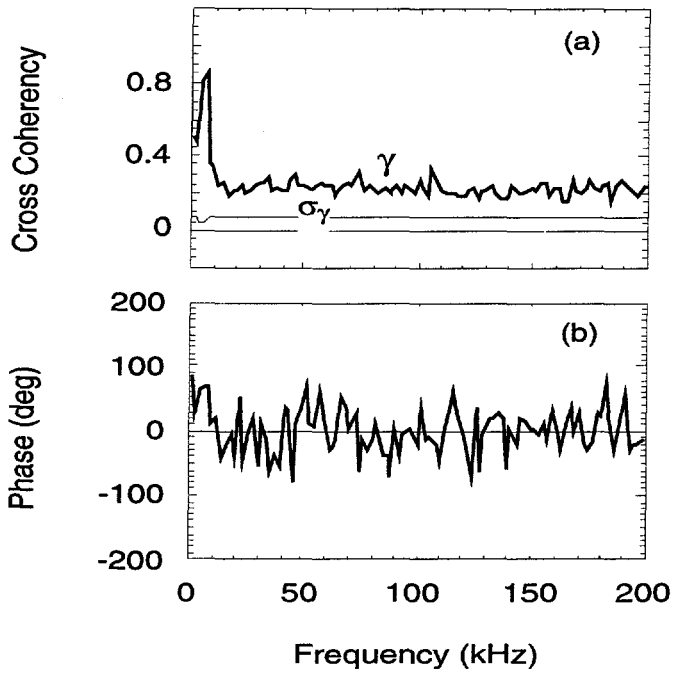

Figure 7. Cross-coherence (a) and phase shift (b) between the fluctuations of the radial magnetic field and parallel electron heat flux in CCT tokamak at the probe radial position of 29 cm. The statistical noise level of the cross-coherence is shown by the thin solid line.

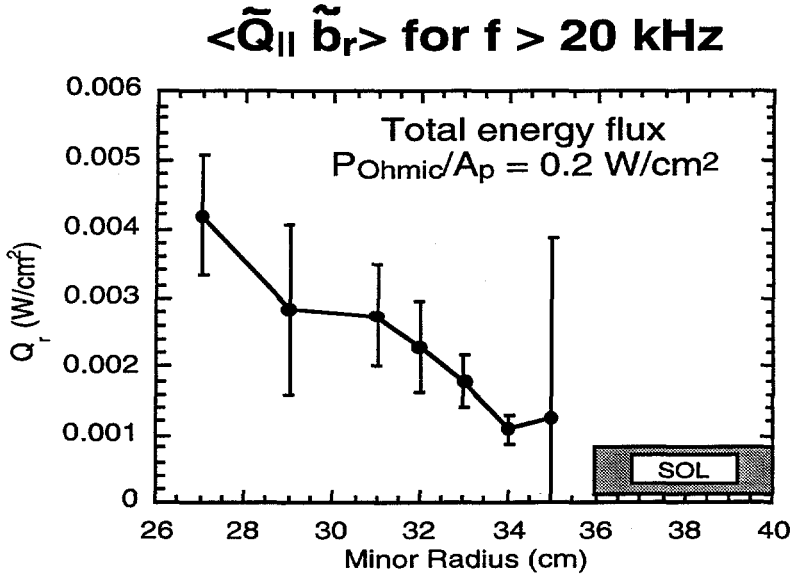

Figure 8. Radial profile of broadband turbulent (f > 20 kHz) magnetic heat transport in CCT tokamak. $Q_r = \frac{<\tilde{Q}_{||}\tilde{B}_r>}{B}$. The total energy flux $P_{Ohmic}/A_p = 0.2\ W/cm^2$.

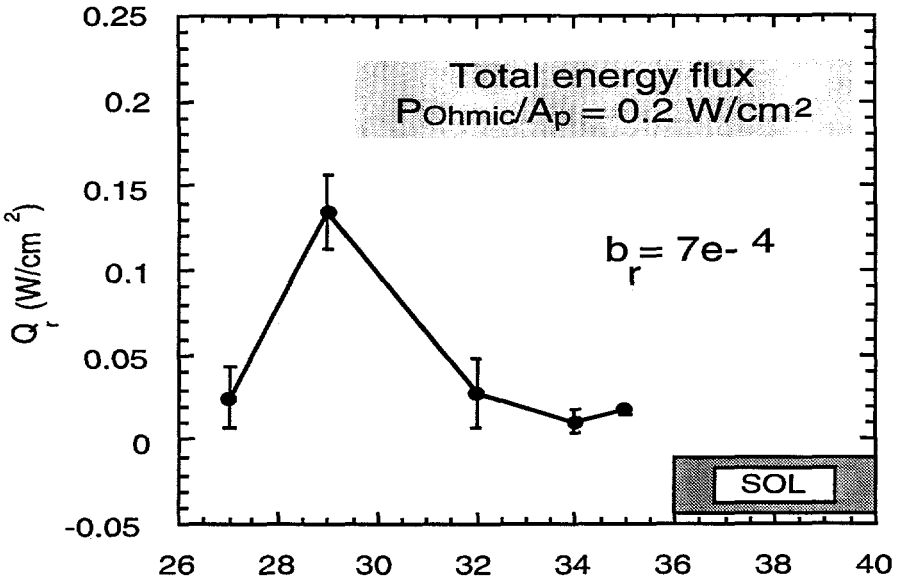

Figure 9. Radial profile of the total magnetic heat transport $Q_r = \frac{\langle \tilde{Q}_{\|} \tilde{B}_r \rangle}{B}$ at the amplitude of the radial magnetic field fluctuation $\tilde{B}_r / B_0 = 7 \times 10^{-4}$. The total energy flux $P_{Ohmic}/A_p = 0.2\ W/cm^2$.

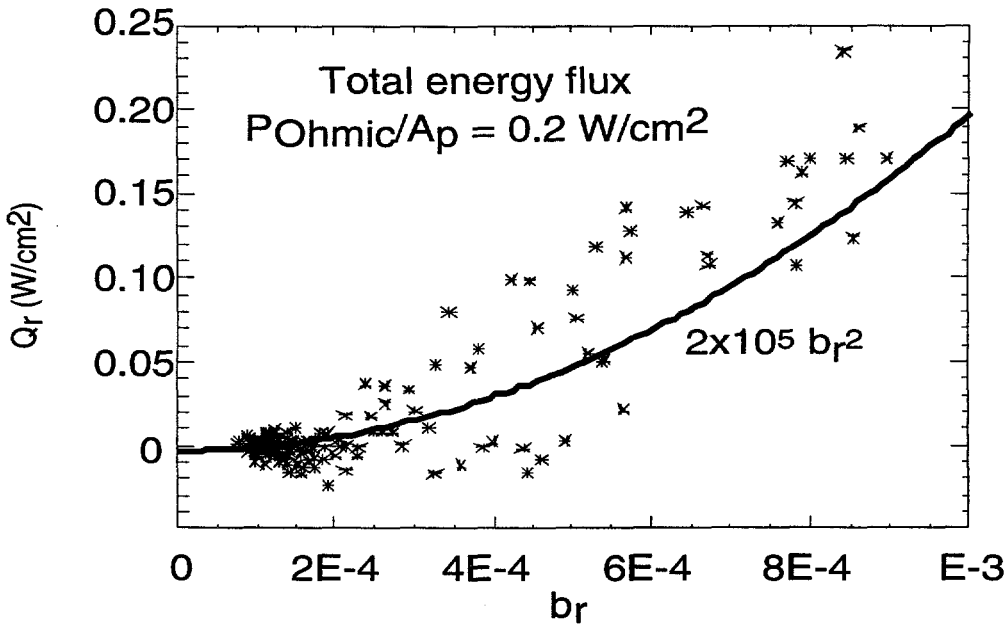

Figure 10. Amplitude of the magnetic fluctuation induced heat flux measured at the radius of the maximum heat transport vs. magnetic field fluctuation amplitude $\tilde{b}_r$. The total energy flux $P_{Ohmic}/A_p = 0.2\ W/cm^2$.

It is instructive to compare this dependence with a prediction of the RR model. Evaluating the radial heat flux at the probe location $Q_r = n_e \nabla T_e v_e L_c \tilde{b}_r^2$ with the density and temperature profiles $n_e = 4\times10^{12}(1-r^2/a^2)$ c m^{-3}, and $T_e = 150(1-r^2/a^2)$ eV yields $Q_r\ [\mathrm{W/cm^2}] = 2\times10^5 \tilde{b}_r^{\,2}$, which is shown in solid line in Fig. 10. The agreement with the experimental data is quite surprising, given our initial assumption that a single 2/1 island is residing at this location and the RR model describes diffusion in a stochastic magnetic field. However, it is conceivable that the non-linear interaction with other ambient modes leads to a stochastic field in the separatrix layer.

Measurements in TEXT-U tokamak are described in Ref. [17]. TEXT-U is a medium sized tokamak with plasma major radius R = 1.05 m and minor radius a = 0.27 cm. For the results presented here, the toroidal field B_T = 2.0 T, the plasma current I_p= 200 kA and the central chord average plasma density n_e= 2x10^{19} m^{-3}. The pyrobolometer was mounted on the top of the tokamak, displaced 90° toroidally from the limiters in the plasma current direction. The front edge of the pyrobolometer was located at the same radial location as the limiters (r = 0.27 m), with the entrance aperture area located 13 mm further out (at r = 0.283 m) where the local measurements of temperature and density are $T_e \approx 30$ eV and $n_e \approx 2\times10^{18}$ m^{-3}.

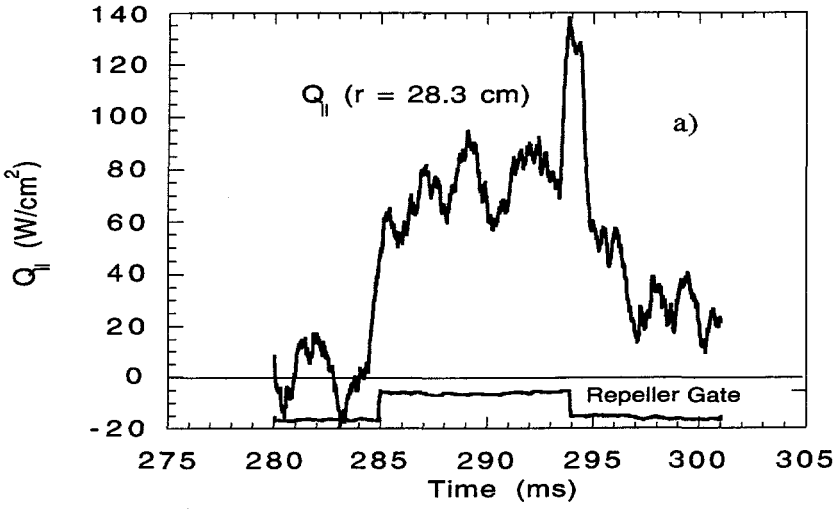

Figure 11. Equilibrium (1 ms averaging) parallel heat flux in TEXT-U. The repeller gating pulse shows the time window of the measurements. The radial position of the bolometer was r = 28.3 cm.

The waveform of $Q_{\|}$ is shown in Fig. 11. Due to a strong high frequency electrostatic noise interference we were unable to resolve high frequency components of the parallel heat flux and only the equilibrium component of it could be reliably measured in the frequency bandwidth of ~1 kHz. Nevertheless it is possible to estimate an upper bound of the radial heat flux was made. To do this, the following substitutions into Eq. 2 were made: $\gamma(f) \equiv 1$, $\cos[\phi(f)] \equiv 1$, $\sum_f |\tilde{Q}_{\|}(f)||\tilde{B}_r(f)| = \overline{Q}_{\|} B_r^{rms}$. After the substitutions $Q_{r\max} = Q_{\|0}\tilde{B}_r^{rms} / B$. For B = 2.0 T, $Q_{\|}$ = 80 x 10^4 W/m^2, and $\tilde{B}_r^{rms}$ = 2x10^{-5} T it is found that Q_{rmax} = 8x10^{-8} W/m^2. This is much less than the loss rate at the last closed flux surface, P_{Ohm} /A_s = 1x10^{-4} W/m^2, estimated from the input Ohmic power reduced by radiation and charge exchange losses. However our measurements were made 13 mm behind the limiter so that the total perpendicular energy flux is reduced from the 10^{-4} W/m^2 by parallel flow to the limiters. Measurements of density and temperature scale lengths [20-30 mm] and infrared camera measurements of the limiter temperature give a scale length for power loss of 10 mm. Therefore, the total perpendicular energy flux at the location of the pyrobolometer is of the order 0.3 x 10^{-4} W/m^2. This is still about factor of 400 larger than the maximum electron thermal flux associated with magnetic fluctuations (8 x10^{-8} W/m^2).

V. Discussion

An intriguing aspect of the observations is that electron heat transport in MST is described by Eq. (1), but with the speed of thermal ions replacing that of electrons. It suggests the existence of an ambipolar constraint. Ambipolar constraints in magnetic turbulence are expected for particle losses *but not for heat losses*, provided the fluctuations are localized in the plasma away from material surfaces [26]. Heat loss can avoid ambipolar constraints because it can be driven by turbulence-induced exchanges of different energy electrons, with no change in potential [27].

There is however, a mechanism (one that is usually neglected in transport calculations) that naturally leads to ambipolar constraints in magnetic fluctuation induced heat transport [28]. This mechanism involves the development of strong, long-lived correlations at small scales among particles moving along turbulent magnetic fields. The occurrence of this clumping is a simple consequence of the spatial correlation properties of exponentially separating magnetic fields. Electrons following neighboring fields remain correlated for longer than those following widely separated fields. There are thus correlations of electrons moving ballistically along the field, with lifetimes that exceed the turbulent correlation time, if the spatial extent of the clump is sufficiently small. These long-lived, localized charge aggregates cannot be included in the plasma dielectric response; consequently they create a wake or emission field as they move ballistically. The emission

process, and the subsequent collisionless Landau damping of the emission field, represent the turbulent energy and momentum exchange mechanism between particles that allows for irreversible heat loss. Because the wake field is resonantly excited by emission and resonantly damped by Landau damping, the energy and momentum exchange mimics collisional transport, where like-particle collisions lead to no transport, except for the heat exchanged in the presence of a temperature gradient. The latter situation provides a non ambipolar-constrained component of the electron heat flux. Emission by electron clumps, with subsequent damping of the emission field on the ion distribution leads to an ambipolar-constrained component [29].

The relative size of these components depends on the spectrum of $\tilde{b}_k^2$ as a function of $k_{||}$ in the frequency range for which transport occurs. If $\tilde{b}_k^2$ (for $\omega < 20$ kHz) peaks about $k_{||} = 0$, the self-consistent electron heat loss in magnetic turbulence is described by Eq. (1). If $\tilde{b}_k^2$ (for $\omega < 20$ kHz) peaks at $k_{||} = k_o \neq 0$ and there is no power at $k_{||} = 0$ ($k_o - \Delta k_{||}/2 > 0$, where $\Delta k_{||}$ is the spectrum width), the transport goes as

$$Q_e \cong -v_i \frac{1}{L_{ni}} \frac{\tilde{b}^2/B_o^2}{k_o} \frac{1}{\pi^{1/2}} \frac{\omega^2}{v_i^2 k_o^2} \left(1 + \frac{\omega}{\omega_{*e}}\right) \left(2 - k_\perp^2 \rho_i^2\right) \left(1 - \frac{\Delta k_{||}^2}{4k_o^2}\right)^{-2}, \quad (3)$$

where v_i is the ion thermal velocity, L_{ni} is the ion temperature gradient scale length, ω is the frequency of the magnetic turbulence, ρ_i is the ion gyroradius, and ω_{*e} is the electron diamagnetic frequency.

In the edge of MST, where the heat flux is measured, Eq. (3) applies. There, the parallel wavenumbers of the resonant tearing modes that dominate transport ($\omega < 20$ kHz) are large ($k_{||} \sim$ 1-2 m^{-1}) because they are centered on distant rational surfaces deep in the core. Locally resonant modes have high frequency ($\omega \sim 100$ kHz) and therefore make no contribution to transport. Taking ω as the rotation frequency of the core plasma (where the tearing modes are resonant) relative to the edge (where the measurement is made), the factor $\omega^2/v_i^2k_o^2$ is close to unity. The other factors are also close to unity and Eq. (3) becomes comparable to Eq. (1), but with the ion thermal velocity in place of the electron thermal velocity. Because the peak of the spectrum must shift to $k_{||} = 0$ in moving from the edge to the core, it is expected that core electron heat transport in MST will satisfy Eq. (1). Note that this aspect of MST transport is at least superficially similar to the CCT result, where Eq. (1) holds at the resonant surface, but overestimates the flux away from the resonant surface. The same mechanism could account for transport in both machines, if the magnetic fluctuation spectrum in CCT is produced by larger amplitude fluctuations at low order surfaces [such as the (2,1) surface], with much smaller amplitude fluctuations on higher order surfaces away

from the low order surfaces. However, it is more likely that the CCT results simply reflect the fact that the magnetic field ceases to be stochastic away from the (2,1) surface.

VI. Conclusions

In summary, we have directly measured the electron energy transport induced by magnetic fluctuations in the RFP and tokamak. We have demonstrated that a technique, based on the development of a fast, insertable bolometer, can be applied to the edge of different plasma experiments to similarly discover the contribution of magnetic fluctuations to transport. Measurement of the correlation between fluctuations of the parallel heat flux $\tilde{Q}_{||}$, and the radial magnetic field $\tilde{B}_r$, give a definitive measure of the magnetic fluctuation induced heat transport.

For the RFP we have demonstrated that magnetic fluctuations can drive significant energy transport. This demonstration is definitive since we have directly measured the energy flux driven by magnetic fluctuations. The radial profile and frequency dependence of the fluctuation induced flux is in accord with the expectation that internally resonant tearing oscillations are responsible for the transport. In the extreme edge, where the tearing oscillations do not break magnetic surfaces, the energy flux from magnetic fluctuations is small. It is worth noting that the RFP concept might be in the unique position of being accompanied by a basic understanding of the origin of both the dominant fluctuations and the anomalous energy transport. This feature is subject to the caveat that the results reported here were limited to one device under restricted conditions. Nonetheless, a physics basis now exists for the control of fluctuations and transport in the RFP, and appropriate techniques are presently being formulated.

An intriguing aspect of the observations is that electron heat transport in RFP is described by Rochester-Rosenbluth stochastic diffusion model, but with the speed of thermal ions replacing that of electrons.

The magnetic fluctuation induced heat flux was also measured in the edge plasma of tokamaks. The basic conclusion is that transport is small and magnetic fluctuations are not the cause of anomalous transport in tokamaks such as CCT and TEXT-U. It was concluded in Ref. [4] that electrostatic energy transport dominates at the tokamak plasma edge. There is, of course, always a possibility that very short wavelength fluctuations outside the measurement range could play a role, or that under other conditions, such as high beta, magnetic fluctuations become significant.

For the discharges in which $m = 2$ Mirnov oscillations are large, we observe that the energy flux from magnetic fluctuations can become as large as the total energy flux in the vicinity of the $q = 2$ surface, and over a radial range about equal to the calculated island width. This provides a strong indication of magnetic island induced transport. It is also in agreement with experiments with externally controlled static magnetic stochasticity [30] in the

TEXT-U tokamak. Given the overlap of magnetic islands this mechanism can be responsible for the total energy transport as it was implied in Ref. [8, 9].

Acknowledgments.

The authors appreciate discussions with and assistance of many MST, CCT, and TEXT-U group members. This work was supported by the US. Department of Energy.

References

1 P.C. Liewer, Nucl. Fusion **25**, 543 (1989).
2. J.D. Callen, Phys Rev. Lett. **39**, 1540 (1977).
3. A.B. Rechester and M.N. Rosenbluth, Phys. Rev. Lett. **40**, 38 (1978).
4. Ch.P. Ritz, R.V Bravenec, P.M. Schoch, R.D. Bengtson, et.al, Phys. Rev. Lett. **62**, 1884 (1989).
5. S.J. Zweben, R.J. Taylor, Nucl. Fusion **21**, 193 (1981);
6. D.E. Graessle, S.C. Prager, and R.N. Dexter,Phys. Fluids B **3**, 2626 (1991).
7. D.W. Swain, M. Murakami, S.C. Bates, S.C. Bush, et.al, Nucl. Fusion **21**, 1409 (1981).
8. N. Ohyabu, G.L. Jans, R.D. Stambough, and E.J. Strait, Phys. Rev. Lett. **58**, 120 (1986).
9. M. Malacarne, P.A. Dureprex, Nuclear Fusion **27**, 2113 (1987).
10 R.N. Dexter *et al.*, Fusion Technology **19**,131 (1991)
11. R.J. Taylor, M.L. Brown, B.D. Fried, et. al., Phys. Rev. Lett. **63**, 2365 (1989).
12 K.W. Gentle, Nucl. Technol. Fusion **1**, 479 (1981)
13. S.C. Prager, Plasma Phys. Controlled Fusion **32**, 903 (1990).
14. G. Fiksel, J. Frank, and D. Holly, Rev. Sci. Instrum. **64**, 2761, (1993).
15. G. Fiksel, Rev. Sci. Instrum. **66**, 662 (1995).
16. G. Fiksel, S.C. Prager, W. Shen, and M. Stoneking, Phys. Rev. Lett. **72**, 1028 (1993).
17. G. Fiksel, R.D. Bengtson, S.C. Prager, and A.J. Wooton, Phys. Plasmas **2** (12), 1995.
18 G. Fiksel, S.C. Prager, P. Pribyl, R.J. Taylor, and G.R. Tynan, Phys.Rev. Lett, **75**, 3866 (1995).
19 A.F. Almagri *et al.*, Phys. Fluids B **4**, 4080 (1992).
20 J.S. Sarff *et al.*, Phys. Fluids B **5** 2540 (1993).
21 S. Assadi, S.C. Prager, and K.L. Sidikman, Phys. Rev. Lett. 69, 281 (1992).
22 J.S. Sarff, A.F. Almagri, M. Cekic, C.-S. Chaing, D. Craig, D.J. Den Hartog, G. Fiksel, S.A. Hokin, R.W. Harvey. H. Ji, C. Litwin, D. Sinitsin, C.R. Sovinec, J.C. Sprott, and E. Uchimoto, Phys, Plasmas **2**, 2440 (1995).
23 D.D. Schnack, D.C. Barnes, Z. Mikic, D.S. Harned, and E.J. Caramana, Journ. Comput. Phys. **70**, 330 (1987).
24 M.R. Stoneking, G. Fiksel, S.A. Hokin, S.C. Prager, and H. Ji, Rev. Sci. Instrum, **66**, 812 (1995)
25 S. Hokin, *et. al.*, Journal of Nuclear Fusion, **12** (3), 281 (1993).
26 R.E. Waltz, Phys. Fluids **25**, 1269 (1982).
27 A.A. Thoul, P.L. Similon, and R.N. Sudan, Phys. Plasmas **1**, 601 (1994).
28 P.W. Terry and P.H. Diamond, Phys. Fluids B **2**, 1128 (1990).
29 P.W. Terry, *et al.*, Phys. Plasmas **3**, 1999 (1996).
30. A.J. Wooton, S.C. McCool, S.-B. Zheng, Fusion Technol, **19**, 473 (1991).

EXTERNAL DISTRIBUTION IN ADDITION TO UC-20

S.N. Rasband, Brigham Young University
R.A. Moyer, General Atomics
J.B. Taylor, Institute for Fusion Studies, The University of Texas at Austin
E. Uchimoto, University of Montana
F.W. Perkins, PPPL
O. Ishihara, Texas Technical University
M.A. Abdou, University of California, Los Angeles
R.W. Conn, University of California, Los Angeles
P.E. Vandenplas, Association Euratom-Etat Belge, Belgium
Centro Brasileiro de Pesquisas Firicas, Brazil
P. Sakanaka, Institute de Fisica-Unicamp, Brazil
Mme. Monique Bex, GANIL, France
J. Radet, CEN/CADARACHE, France
University of Ioannina, Greece
R. Andreani, Associazione EURATOM-ENEA sulla Fusione, Italy
Biblioteca, Istituto Gas Ionizzati, EURATON-ENEA-CNR Association, Italy
Plasma section, Energy Fundamentals Division Electrotechnical Laboratory, Japan
Y. Kondoh, Gunma University, Kiryu, Gunma, Japan
H. Toyama, University of Tokyo, Japan
Z. Yoshida. University of Tokyo, Japan
FOM-Instituut voor Plasmafysica "Rijnhuizen," The Netherlands
Z. Ning, Academia Sinica, Peoples Republic of China
P. Yang, Shandong University, Peoples Republic of China
S. Zhu, University of Science & Technology of China, People's Republic of China
I.N. Bogatu, Institute of Atomic Physics, Romania
M.J. Alport, University of Natal, Durban, South Africa
R. Storer, The Flinders University of South Australia, South Australia
B. Lehnert, Royal Institute of Technology, Sweden
Librarian, CRPP, Ecole Polytechnique Federale de Lausanne, Switzerland
B. Alper, Culham Laboratory, UK
A. Newton, UK

2 for Chicago Operations Office
5 for individuals in Washington Offices

INTERNAL DISTRIBUTION IN ADDITION TO UC-20
80 for local group and file